BNL-108605-2015-JA

Interactions of a potent cyclic peptide inhibitor with the light chain of botulinum neurotoxin A: insights from x-ray crystallography

Desigan Kumaran, Michael Adler, Matthew Levit, Michael Krebs, Richard Sweeney, Subramanyam Swaminathan

Accepted to the Journal of Bioorganic & Medicinal Chemistry

October 2015

Biology Department

Brookhaven National Laboratory

U.S. Department of Energy

Notice: This manuscript has been authored by employees of Brookhaven Science Associates, LLC under Contract No. DE- SC0012704 with the U.S. Department of Energy. The publisher by accepting the manuscript for publication acknowledges that the United States Government retains a non-exclusive, paid-up, irrevocable, world-wide license to publish or reproduce the published form of this manuscript, or allow others to do so, for United States Government purposes.

DISCLAIMER

This report was prepared as an account of work sponsored by an agency of the United States Government. Neither the United States Government nor any agency thereof, nor any of their employees, nor any of their contractors, subcontractors, or their employees, makes any warranty, express or implied, or assumes any legal liability or responsibility for the accuracy, completeness, or any third party's use or the results of such use of any information, apparatus, product, or process disclosed, or represents that its use would not infringe privately owned rights. Reference herein to any specific commercial product, process, or service by trade name, trademark, manufacturer, or otherwise, does not necessarily constitute or imply its endorsement, recommendation, or favoring by the United States Government or any agency thereof or its contractors or subcontractors. The views and opinions of authors expressed herein do not necessarily state or reflect those of the United States Government or any agency thereof.

Interactions of a potent cyclic peptide inhibitor with the light chain of botulinum neurotoxin A: insights from x-ray crystallography

Desigan Kumaran[†], Michael Adler[‡,*], Matthew Levit[‡], Michael Krebs[‡], Richard Sweeney[§], Subramanyam Swaminathan[‡]

[†]Biological, Environmental & Climate Sciences Department, Brookhaven National Laboratory, Upton, NY 11973, United States

[‡]Analytical Toxicology Division, U.S. Army Medical Research Institute of Chemical Defense (USAMRICD), Aberdeen Proving Ground, MD 21010, United States

[§]Research Division, USAMRICD, Aberdeen Proving Ground, MD 21010, United States

*Corresponding author, email: michael.adler2.civ@mail.mil

Abstract

The seven antigenically distinct serotypes (A to G) of botulinum neurotoxin (BoNT) are responsible for the deadly disease botulism. BoNT serotype A (BoNT/A) exerts its lethal action by cleaving the SNARE protein SNAP-25, leading to inhibition of neurotransmitter release, flaccid paralysis and autonomic dysfunction. BoNTs are dichain proteins: the heavy chain is responsible for neurospecific binding, internalization and translocation, and the light chain is responsible for substrate cleavage. Because of their extreme toxicity and prior history of weaponization, the BoNTs are considered to be potential bioterrorism agents.

No post-symptomatic therapeutic interventions are available for BoNT intoxication other than critical care; therefore it is imperative to develop specific antidotes against this neurotoxin. To this end, a cyclic peptide inhibitor (CPI-1) was synthesized and found to inhibit BoNT/A light chain (Balc) with high affinity. When tested in a cell-free Förster resonance excitation transfer (FRET) assay, CPI-1 was found to have a K_i of 13.9 nM using full-length Balc448 and 42.1 nM using a truncated crystallizable form of light chain (Balc424). Co-crystallization of CPI-1 with Balc424 revealed that in the Balc-CPI-1 complex, the inhibitor adopts a helical conformation, occupies a high percentage of the active site cavity and interacts in an amphipathic manner with critical active site residues. The data suggest that CPI-1 prevents SNAP-25 from accessing the Balc active site by blocking both the substrate binding path at the surface and the Zn^{2+} binding region involved in catalysis. This is in contrast to linear peptide inhibitors described to date which block only the latter.

Abbreviations: BoNT, botulinum neurotoxin; Balc, botulinum neurotoxin A light chain; Balc424, Balc truncated at residue 424; Balc448; full-length Balc, CPI-1, cyclic peptide inhibitor-1; CPI-2, cyclic peptide inhibitor-2; FRET, Förster resonance energy transfer; HBAT, hepatavalent botulism antitoxin; LC, light chain; PLM, peptide-like molecule; SNARE, soluble N-ethylmaleimide-sensitive fusion protein attachment protein receptor; SNAP-25, synaptosome-associated protein of 25 kDa; TCEP, tris (2-carboxyethyl)phosphine; TPI, tetra peptide inhibitor; VAMP1/2, vesicle-associated membrane protein isoforms 1 or 2.

I. Introduction

Botulinum neurotoxins (BoNTs), the most poisonous substances known to human kind, are the causative agents of botulism, a life-threatening neuroparalytic disease. The BoNTs are produced by Gram-positive spore-forming anaerobic bacteria of the genus *Clostridium* and are members of a family of clostridial neurotoxins that also include tetanus toxin.[1] There are seven confirmed serotypes of BoNT (A to G), which share significant similarity in sequence, structure and function.[2-4] Of these, BoNT/A, B, E and, to a lesser extent, F have been implicated in human botulism with BoNT/A being the most potent and persistent. BoNTs are synthesized as single chain protoxins of ~150 kDa and undergo conversion to the bioactive disulfide-linked dichain molecules (holotoxins) after proteolytic cleavage by unidentified proteinases.[5-7] The dichain consists of a heavy chain and light chain (LC) with molecular masses of ~100 kDa and ~50 kDa, respectively. The heavy chain contains two distinct domains: the N-terminal translocation domain and C-terminal receptor binding domain.

At the neuromuscular junction, the BoNTs bind to specific receptors at the motor neuron terminal and are internalized into endosomes. Following endosomal acidification, the translocation domain forms channels across the endosomal membrane, which allow the LC to escape into the cytosol. BoNT LCs are Zn^{2+} metalloproteases, and they specifically cleave one of three SNARE proteins (synaptosome-associated protein of 25 kDa (SNAP-25), vesicle-associated membrane protein, isoform 1 or 2 (VAMP-1/2) and syntaxin) that are required for synaptic vesicle fusion and transmitter release. In particular, BoNTs block the release of the neurotransmitter acetylcholine and cause flaccid paralysis that can be fatal if the respiratory muscles become sufficiently compromised.[8-10] BoNT/A and /E cleave SNAP-25, BoNT/B, /D, /F and /G cleave VAMP1/2, and BoNT/C cleaves both SNAP-25 and syntaxin.[11-16]

BoNTs have been designated as potential biowarfare/bioterrorism agents since they are highly toxic, easily concealed and can disrupt critical infrastructure required for the functioning of society.[17] Moreover, the recent prominence of BoNTs in clinical and aesthetic use increases the risk of mishandling and accidental overdose. The currently approved medical countermeasure for adult botulism is a despeciated heptavalent equine antitoxin (HBAT), which is effective in the early stages of the disease, before lethal quantities of circulating toxin become internalized (generally 24 to 48 h following exposure).[18-19] Management of intoxicated patients requires a high level of critical care over an extended period, often involving mechanical ventilation. This level of care may not be possible in a mass casualty situation.[17] Therefore, it is imperative to develop pharmacological treatments for BoNT intoxication that are effective in symptomatic individuals without the constraint of a short time window. This can be accomplished by therapeutic agents able to enter the nerve terminal and inhibit the internalized BoNT LC.[18]

Inhibitors of BoNT/A-mediated cleavage of SNAP-25 generally act by preventing the binding of substrate to the active site of the BoNT/A LC (Balc). To this end we discovered various tetra-peptide inhibitors (TPIs) against Balc protease action using structure- and substrate-based drug design approaches and derived a pharmacophore model to aid in the development of more potent inhibitors.[20,21] In addition, we and others have also developed various peptidomimetics, hydroxamate-based inhibitors, peptide-like-molecules (PLMs) and small molecule non-peptide inhibitors.[20-27] Unfortunately, these compounds did not possess robust *in vivo* efficacy.

In this study, we report on a new cyclic peptide inhibitor (CPI-1), focusing on the crystal structure of a tight complex between CPI-1 and a truncated crystallizable form of the LC

(Balc424), at near-atomic resolution. CPI-1was found to be a highly potent BoNT/A inhibitor, exhibiting a K_i = 13.9 ± 1.7 nM with Balc448 and 42.1 ± 4.6 nM with Balc424. The complex crystal structure of CPI-1 and Balc424 revealed new molecular targets at the Balc424 active site for inhibitor interaction and provided insight into the high potency of CPI-1. This information should facilitate development of effective drugs against botulism that target the active site of the internalized LC.

2. Materials and methods

2.1. Synthesis of inhibitors

Cyclic peptide inhibitors DAB(C)-RWTKCL-NH_2 (CPI-1) and DAB(C)-RWTKC-NH_2 (CPI-2) were synthesized by AnaSpec, Inc., Fremont, CA, USA or Quality Phytochemicals, LLC, East Brunswick, NJ, USA. The peptides were >95% pure as determined by high performance liquid chromatography (HPLC). DAB(C) denotes Cys coupled to the 4-amino group of 2,4-diaminobutanoic acid (DAB) by an amide bond. The cyclic structure of CPI-1 was confirmed independently by NMR and mass spectrometry (Soni, Oyler, Housman and Adler, unpublished observations).

2.2. Cloning, expression and purification of Balc424

Balc424 was cloned, over-expressed in *E. coli* and purified to homogeneity using nickel affinity chromatography followed by size exclusion chromatography, as described previously.[28] The purified enzyme in 20 mM HEPES, 2 mM dithiothreitol, 200 mM NaCl (pH 7.4) was concentrated to 10 mg/ml and stored at −80 °C until use. Balc448 was a gift from Dr. Leonard Smith, U.S. Army Medical Research Institute of Infectious Diseases, Fort Detrick, MD, USA.

2.3. BoTest® A/E FRET assay

Fluorescence measurements were made on a Spectramax M5 microplate reader (Molecular Devices, LLC, Sunnyvale, CA, USA). To determine inhibitor efficacy, we performed kinetic studies using Balc424 or Balc448 and a FRET reporter substrate (BoTest® A/E [CFP-SNAP-$25_{141-206}$-YFP; BioSentinel Pharma LLC, Madison, WI, USA]). Reactions were carried out in 96-well opaque black Microfluor 1 plates (ThermoFisher Scientific, Waltham, MA, USA) in triplicate, in buffer containing 50 mM HEPES pH 7.1, 0.1% Tween-20, 10 µM $ZnCl_2$ and 0.15% glycerol. CPI-1 was pre-incubated with Balc424 (200 pM) or Balc448 (20 pM) at 37 ^{o}C for 30 min to ensure enzyme-inhibitor equilibrium.

At the end of the pre-incubation time, 0.1 µM BoTest was added, and kinetic measurements were performed at 1 min intervals. Two separate excitation (ex) and emission (em) settings were used: 434 nm ex/470 nm em for CFP fluorescence and 434 nm ex/528 nm em for FRET fluorescence. The reduction in FRET/CFP ratio was determined for each condition in the initial catalytic phase of the reaction. IC_{50} values were obtained via least-squares nonlinear regression fit using Prism v5.04 (GraphPad Software, La Jolla, CA, USA). Conversion of IC_{50} to K_i was made using a public domain IC_{50}-to-K_i-converter (http://botdb.abcc.ncifcrf.gov/toxin/kiConverter.jsp) with a previously established K_m for the BoTest substrate of 0.7 µM.[29]

2.4. Crystallization and x-ray data collection

Balc424 was co-crystallized with CPI-1 by the sitting drop vapor diffusion method at room temperature. Prior to crystallization, a stock solution of CPI-1 was prepared with water and added to the concentrated Balc424 solution (~10 mg/ml). Balc424 was mixed with a 5 to 10

molar excess of CPI-1 for co-crystallization trials. Balc424-CPI-1 inhibitor mixtures were incubated at 4 °C for 1 h.

Better diffracting complex crystals were obtained at the Balc424:peptide molar ratio of 1:7. Crystallization conditions were 23% (w/v) PEG 3350, 0.3 M $(NH_4)_2SO_4$ and 50 mM HEPES, pH 6.5. Crystals appeared after 2 days and were flash-cooled by direct immersion in liquid nitrogen using mother liquor supplemented with 20% (v/v) ethylene glycol. X-ray intensity data were collected at the X29 beam line of the National Synchrotron Light Source (NSLS) using ADSC QUANTUM 315 detector. Crystals diffracted to 1.95 Å and belong to the monoclinic space group $P2_1$ with one molecule in the asymmetric unit. Data were indexed, integrated and scaled using the program HKL2000.[30] Crystal parameters, data collection and refinement statistics are given in Table 1.

2.5. Structure determination and refinement

The crystal structure of the complex was determined by rigid-body refinement followed by restrained refinement of the native structure (Protein Data Bank [PDB] id: 3BWI) using REFMAC.[31,32] The difference Fourier map clearly showed well-defined electron density allowing unambiguous modeling of the inhibitor (see Figure 4). However, to eliminate bias in the electron density, the protein was initially modeled and refined in the absence of the inhibitor. Model building of both the enzyme and inhibitor in the electron density was done using the graphics program COOT.[33] In the structure, residual densities elsewhere were modeled as sulfate ions. The refined models were validated using the Ramachandran plot and the program PROCHECK.[34] The refinement statistics and quality of the model are given in Table 1. The atomic coordinates were deposited in the PBD under accession code 4ZJX.

Table 1. Data collection and refinement statistics

Values for the highest resolution shell are given within parentheses.

Cell Dimensions	a = 51.0Å, b = 66.4Å, c = 64.9Å
	α = 90º, β = 98.5º, γ = 90º
Space Group	P 2_1
Data Collection Statistics	
Resolution limit (Å)	50-1.95 (2.02-1.95)
Unique reflections	28926 (1861)
Completeness (%)	91.8 (59.3)
Rmerge [a] (%)	13.3 (40.4)
$\langle I/(\sigma I)\rangle$	9.3 (2.0)
Redundancy	12.5(6.4)
Refinement statistics	
Resolution (Å)	50.0-1.95
R factor [b] (%)	17.7
Rfree (%)	22.9
Average B-factors ($Å^2$)	
Main chain	30.7
Side chain	33.8
Waters	35.1
Ions	51.4
Cyclic Peptide Inhibitor (CPI-1)	43.3
Root mean square deviations	
Bond distance (Å)	0.019
Bond angles (°)	1.9
Number of atoms	
Proteins	3368
Waters	183
Ions	16
Cyclic Peptide Inhibitor (CPI-1)	69
Ramachandran plot statistics (%)	
Residues in core regions	89.2
Residues in additionally allowed regions	10.3

[a] Rmerge = $\sum_{hkl}\sum_i |I_i(hkl) - \langle I(hkl)\rangle| / \sum_{hkl}\sum_i I_i(hkl)$, where <*I*(*hkl*)> is the average intensity over symmetry equivalents.

[b] R factor = $\sum_{hkl} \left||F_{obs}| - |F_{calc}|\right| / \sum_{hkl} |F_{obs}|$.

3. Results and discussion

3.1. Structure of Balc424 Active Site

The crystal structure of the Balc424 active site in the absence of inhibitor is shown in Figure 1A. As depicted in this surface representation, the active site cavity of Balc424 is unusually large (surface = 18Å x 18Å; depth = 21Å). This may allow significant mobility of small linear peptide inhibitors, leading to weak inhibition

Consistent with this notion, in previous studies, TPIs such as RRGC, RRGL or RRGI (Figure 1B) had a limited ability to inhibit the proteolysis of SNAP-25. [21] It is clear from Figure 1B that these TPIs occupy only a small fraction of the active site cavity and engage in relatively few stabilizing interactions with active site residues. To overcome such limitations, it was felt that a larger peptide with a cyclic structure would results in enhanced binding and greater occupancy of the active site cavity.

The design of this cyclic peptide inhibitor (CPI-1) was based on previously reported complex crystal structures of Balc-QRATKM and Balc-PLMs.[20-22,28] CPI-1 has eight residues of which seven are natural amino acids; the eighth is 2,4-diaminobutanoic acid (DAB), a compound that resembles Lys but has 2 fewer methylene groups in its side chain (Figure 2A). CPI-1 has the sequence C(DAB)RWTKCL and partly mimics the ^{196}NQ-RATKML^{203} region of SNAP-25 (P2-P1-P1′-P2′-P3′-P4′-P5′-P6′ residues) near the Q-R cleavage site.

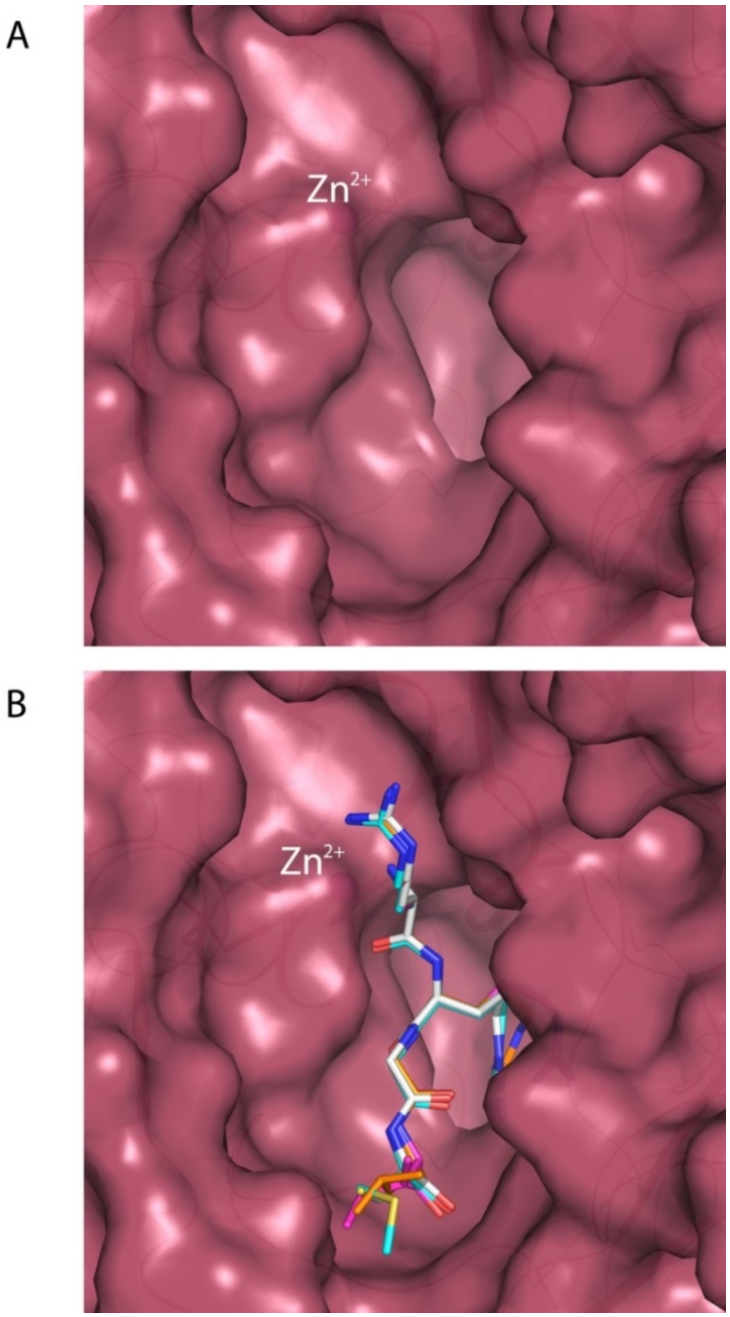

Figure 1. Surface representation of the active site cavity of Balc424. **(A)** Native active site cavity without inhibitor. **(B)** Active site cavity of Balc424 with three superimposed TPIs (RRGC, RRGL and RRGI) shown as stick models.

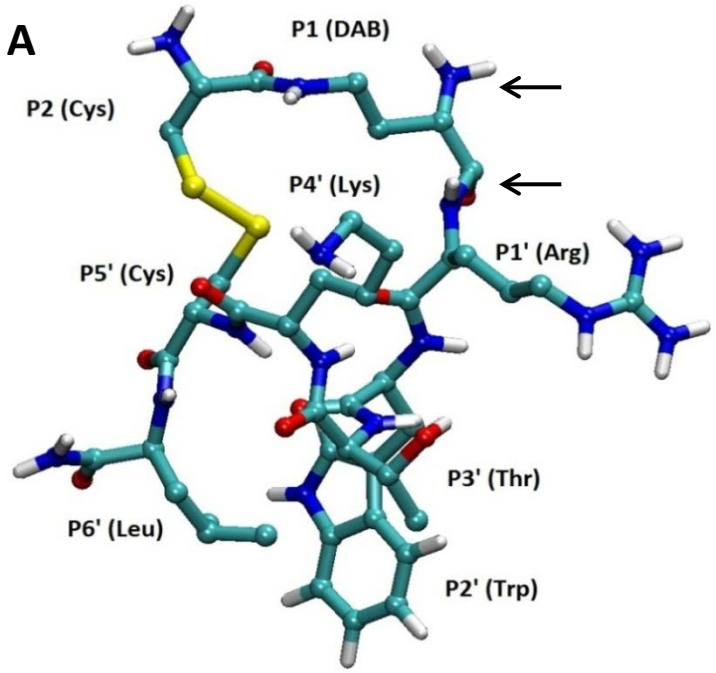
A
P1 (DAB)
P2 (Cys)
P4' (Lys)
P1' (Arg)
P5' (Cys)
P3' (Thr)
P6' (Leu)
P2' (Trp)

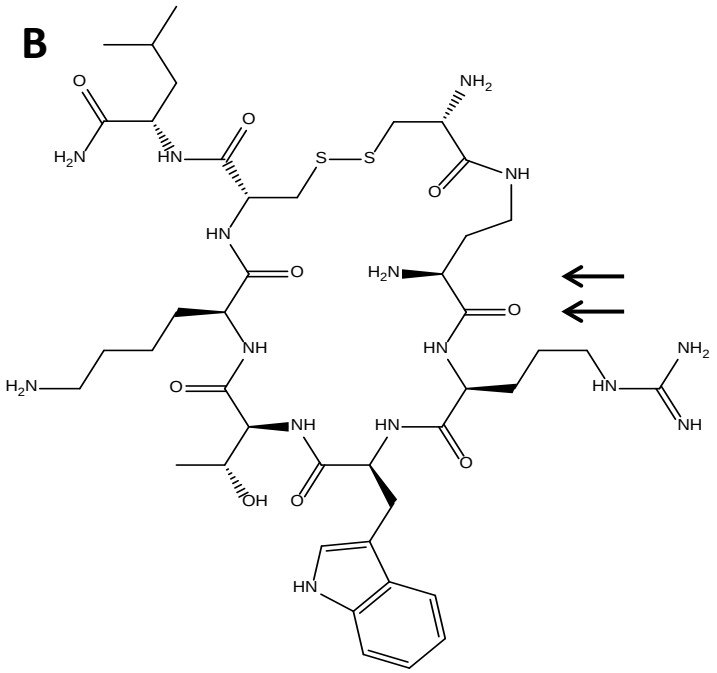
B

Figure 2. CPI-1 structure. **(A)** Stick representation with carbon, oxygen, nitrogen, sulfur and hydrogen atoms colored cyan, red, blue, yellow and white, respectively. **(B)** Standard chemical drawing. The atoms that coordinate the active site Zn^{2+} of Balc424 (carbonyl oxygen and 2-amino nitrogen of DAB) are indicated by arrows.

The sulfhydryl groups of the P2 and P5′ Cys residues form a disulfide bond, making the peptide cyclic. All peptide bonds are conventional except for the one between P2 and P1 residues, where the 4-amino (rather than the 2-amino) group of DAB is coupled to the carbonyl carbon of P2 Cys (Figure 2B). This allows the 2-amino nitrogen and the carbonyl oxygen atoms of DAB to coordinate the active site Zn^{2+}. Effective coordination of this Zn^{2+} is essential for inhibitor activity and is a universal feature of Zn^{2+} metalloprotease inhibitors.[18,20-29]

3.2. Inhibition of Balc by CPI-1

CPI-1 was tested by a Förster resonance energy transfer (FRET) assay using the commercially available reporter CFP-SNAP-$25_{141-206}$-YFP (BoTest® A/E)[29] and either truncated Balc424 or full-length Balc448 (Figure 3). The former was used since it is a crystallizable form of Balc,[20, 21] and the latter, since its sensitivity to inhibitors resembles that of reduced (enzymatically active) BoNT/A holotoxin. CPI-1 inhibited both LCs but was more potent in inhibiting Balc448 (K_i of 13.9 ± 1.7 nM, n = 6) than Balc424 (K_i = 42.1 ± 4.6 nM, n = 6). The K_i of 13.9 nM for Balc448 makes CPI-1 the most potent inhibitor of this LC reported to date. In spite of its high potency, however, CPI-1 would require considerable modification to be considered as a candidate therapeutic agent.

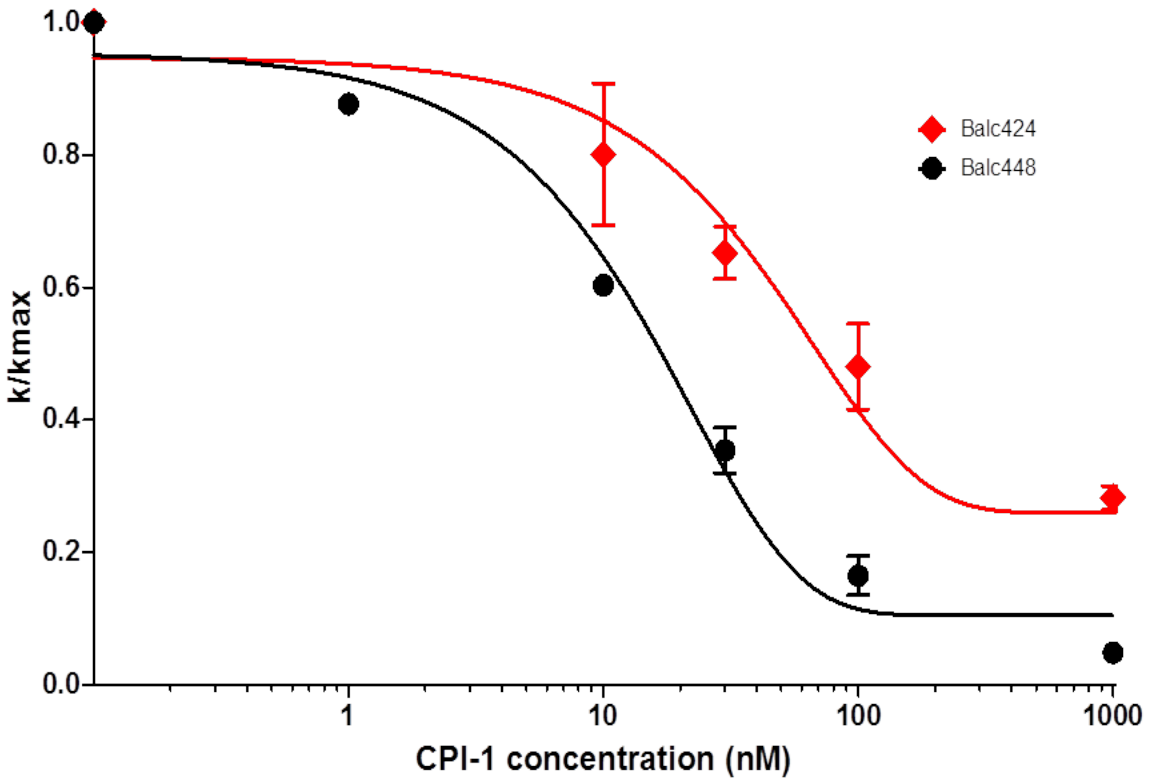

Figure 3. Inhibition of Balc448- or Balc424-mediated cleavage of the FRET reporter CFP-SNAP-$25_{141-206}$-YFP. CPI-1 was incubated with 200 nM Balc424 or 20 pM Balc448 for 30 min at 37 ^{o}C prior to addition of BoTest® A/E. The symbols represent the mean ± SEM of values from 6 experiments. The K_i values for inhibition of Balc448 and Balc424 were 13.9 ± 1.7 nM and 42.1 ± 4.6 nM, respectively.

3.3. Overall Structure of the Balc-Inhibitor Complex

The complex structure of Balc424 with bound CPI-1 was determined by difference Fourier analysis to 1.95 Å resolution. The difference electron density map (Fo-Fc) obtained after rigid body refinement allowed unambiguous modeling of the entire inhibitor molecule (Figure 4).

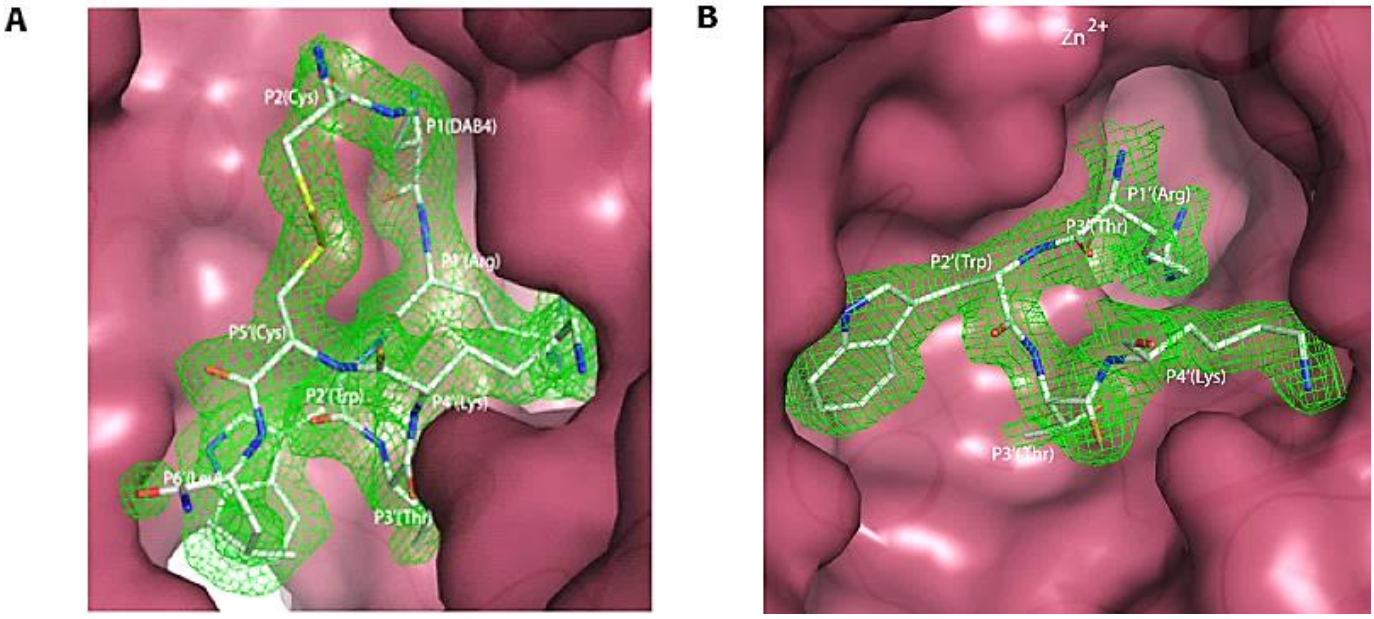

Figure 4. Electron density map for CPI-1. Two different views, **(A)** and **(B)**, are given for the clarity. σ_A-weighted difference electron density ($|F_O|$-$|F_C|$) map contoured at 2.5 σ and overlaid with the refined model of CPI-1. The active site cavity of Balc424 is shown in surface representation (raspberry). Electron density is shown as green mesh, and CPI-1 is depicted as stick model. Grey, red, blue and yellow represent carbon, oxygen, nitrogen and sulfur atoms, respectively.

The overall structure and the conformation of the Zn^{2+}-coordinating residues in the active site of Balc424-CPI-1 complex were essentially the same as those for the native form of the Balc424 crystallized under the same conditions (root-mean-square deviation [RMSD] of ~1.2 Å for 390 common Cα atom pairs). However, the region 247-252, part of the 250 loop, was

disordered and could not be modeled because of a lack of electron density; in the native structure this region formed a well-ordered helix (Figure 5).

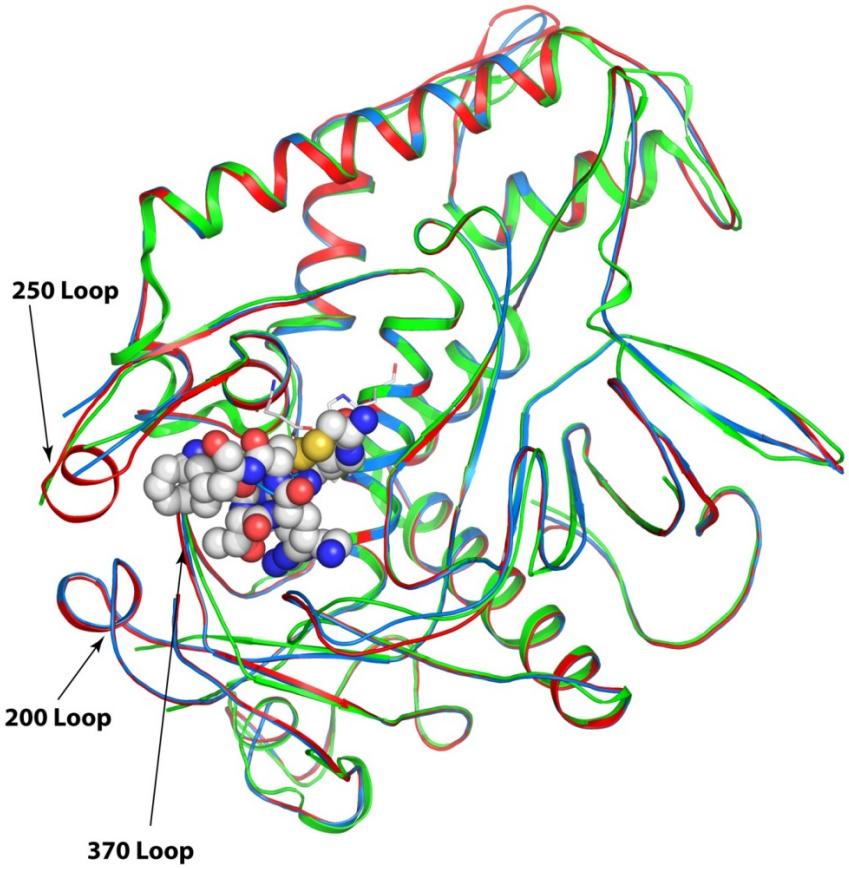

Figure 5. Superposition of native Balc424 structure with its inhibitor-bound structures. Native form of Balc424 (PDB id = 3BWI), CPI-1 bound Balc424 and PLM bound Balc (PDB id = 3DS9) are shown as red, green and blue, respectively. CPI-1 is shown in sphere (CPK) model. Gray, red, blue and yellow represent carbon, oxygen, nitrogen and sulfur atoms, respectively; 200, 250 and 370 loops are indicated with arrows.

Balc424 did not undergo major conformational changes upon binding of inhibitor. This is consistent with our previous findings for TPI-Balc424 complexes[28] but differs from results with PLM-Balc424 cocrystals, where the LC was observed to undergo significant conformational changes in the 60, 250 and 370 loops on binding of inhibitor.[21] CPI-1 binds tightly to the Balc424 active site, adopts a left-handed 3_{10} helical conformation and interacts with 200, 250 and 370 loops (Figure 5).

3.4. Binding and Molecular Interactions

In the Balc424-CPI-1 complex, the free 2-amino group of DAB replaces the nucleophilic water, coordinates with the active site Zn^{2+} and forms a hydrogen bond with the general catalytic base E224 (Figure 6A). Replacement of the nucleophilic water by the 2-amino group of DAB appears to be critical for the inhibitory action of CPI-1 since the former carries out the nucleophilic attack that leads to scission of the bond between Q197 and R198 in SNAP-25.[11] The carbonyl oxygen of DAB forms a hydrogen bond with the side chain hydroxyl of Y366 in addition to coordinating the active site Zn^{2+}. In this complex structure, Zn^{2+} adopts a distorted octahedral geometry by forming four coordination bonds via enzyme residues (H223, H227 and E262) and two via interactions with DAB (carbonyl oxygen and 2-amino nitrogen) (Figure 6A). The free amino group of P2 Cys in CPI-1 forms a hydrogen bond with E164 at the S1 subsite (Figure 6B). A similar interaction with E164 has been identified for Q197 in the P1 position of the SNAP-25 fragment ^{197}Q-RATKM^{202} in the enzyme-substrate complex.[22]

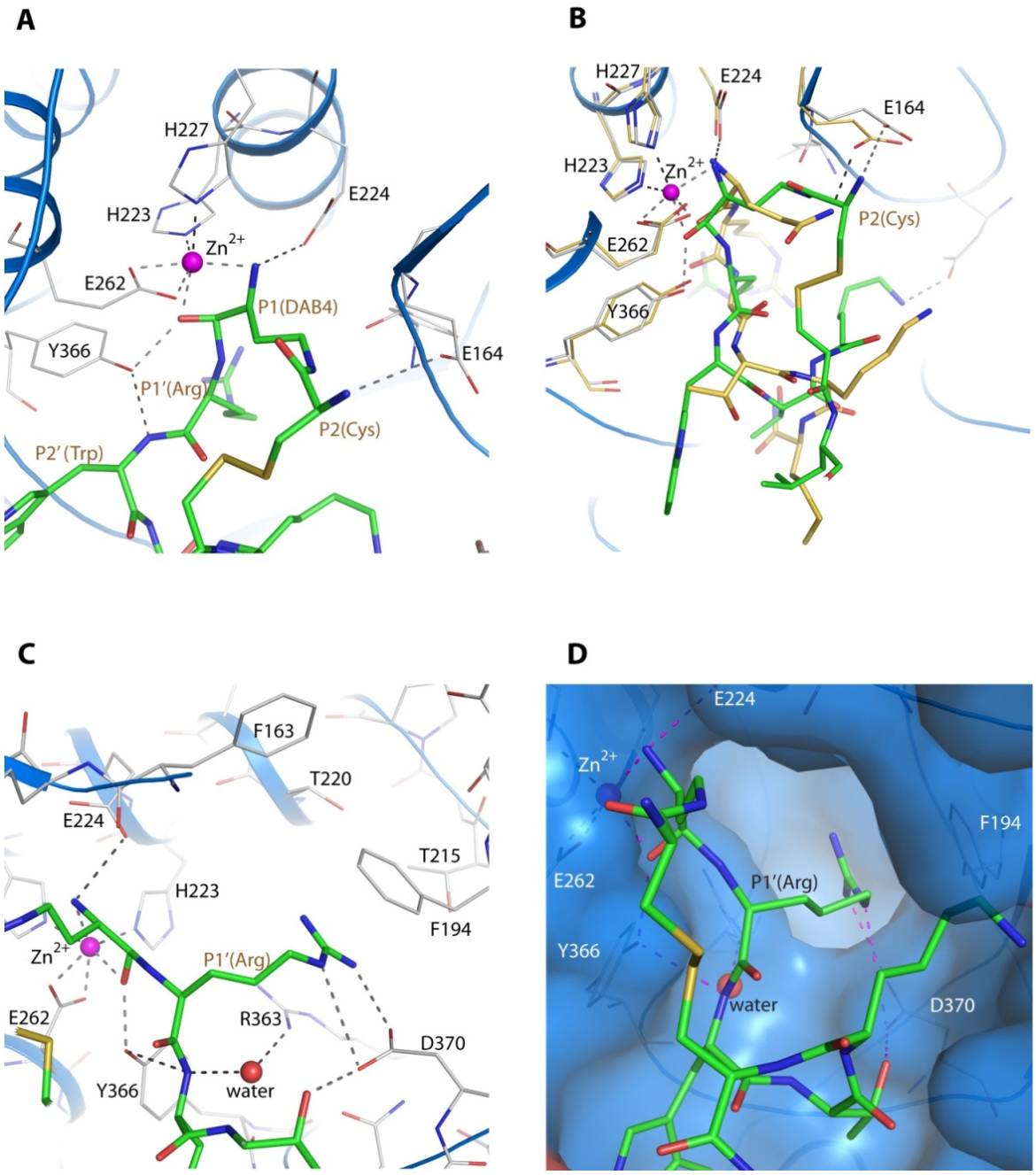

Figure 6. Molecular interactions between CPI-1 and Balc424 at the P1 and P1′ positions. **(A)** Close-up view of the interactions between CPI-1 and Balc424 at the P1 position. **(B)** Superposition of CPI-1 with substrate fragment (^{197}QRATKM^{202}). The bonds and carbon atoms of QRATKM are shown in gold. **(C)** and **(D)** illustrate the interactions

between CPI-1 and Balc424 at the P1′ position. Balc424, CPI-1 and Zn^{2+} are shown in line **(C)** or surface, stick and sphere representations **(D)**, respectively. Water is shown as a red sphere in **(C)** and **(D).** The bonds and carbon atoms of CPI-1 and Balc424 are shown in green and gray, respectively. Magenta, red, blue and yellow represent zinc, oxygen, nitrogen and sulfur atoms, respectively.

The side chain of the P1′ Arg of CPI-1 projects into the S1′ pocket, forms a critical anchoring neighboring point and resides in the S1′ subsite formed by Balc residues D370, T220, T215, R363, F163 and F194 (Figures 6C and 6D). The guanidinium group of P1' Arg forms a salt bridge with D370 and stacks between the phenyl ring of F194 and the guanidinium group of R363. The salt bridge interaction between P1′ Arg and D370 is crucial for substrate cleavage, based on findings that mutation of D370 reduced the catalytic activity of the LC by 250- to 600-fold.[35,36] In addition, the catalytic efficiency of Balc was diminished when R363 and F194 residues were mutated to Ala.[35-37]

Disruption of salt bridge and stacking interactions between substrate and Balc are also important for inhibitor efficacy as indicated in our earlier studies of Balc-inhibitor complex structures involving L-Arg hydroxamate and PLM inhibitors.[21,22,26,28,38,39] In other Balc424-inhibitor complexes with peptides RRATKM, RRGC, RRGI, RRGL, RRGM, RRGF, CRGC and RYGC, the carbonyl oxygen of the P1' Arg was found to be hydrogen bonded to the side chain of R363 directly.[22,28,38] In the Balc424-CPI-1 complex, the carbonyl group of P1' Arg was flipped and was thus unable to interact with R363. Instead, the backbone nitrogen of the P2′ Trp residue engaged in water-mediated interaction with R363.

The amide nitrogen of P1' Arg also interacted with the OH group of Y366 (Figure 6A); Y366 plays a key role in SNAP-25 cleavage as indicated by marked reduction of enzymatic activity when Y366 was mutated to Phe.[36,37] These results suggest that Y366 stabilizes the leaving group as well as the tetrahedral transition state intermediate, where it interacts with the carbonyl oxygen of P1 DAB. Flipping of the peptide backbone between P1' and P2' occurs when the inhibitor has aromatic residues such as Phe or Trp in the P2' position, as observed in the previously reported BALC-RRFC complex.[20,21,38] This flipping is probably due to the strong hydrophobic interaction between the bulky aromatic side chain of the inhibitor and hydrophobic environment of the enzyme.

The active site pocket (S2') of the enzyme at the P2' position is another major binding component of CPI-1. The P2' Trp residue of the inhibitor packs against a cluster of hydrophobic residues of Balc such as V245, L256, V258, Y366, L367 and F369 (Figure 7A). In addition, the nitrogen atom of the indole ring of the P2' Trp interacts with the backbone carbonyl oxygen of E257. These characteristic hydrophobic and hydrogen bond interactions were also observed in the Balc-PLM complex structure[21]. The hydroxyl group of P3' Thr in CPI-1 interacts with D370 of the enzyme through a hydrogen bond, while the 4-methyl group of P3' Thr forms hydrophobic interactions with V70, F369 and F423 (Figure 7B). In the Balc424-PLM complex, the methyl group of P3' Thr forms hydrophobic interactions only with V70.[21] In the complex of Balc with SNAP-25 fragment ^{197}QRATKM^{202}, the hydroxyl group of P3' Thr forms a hydrogen bond with hydroxyl group of Y251.[22]

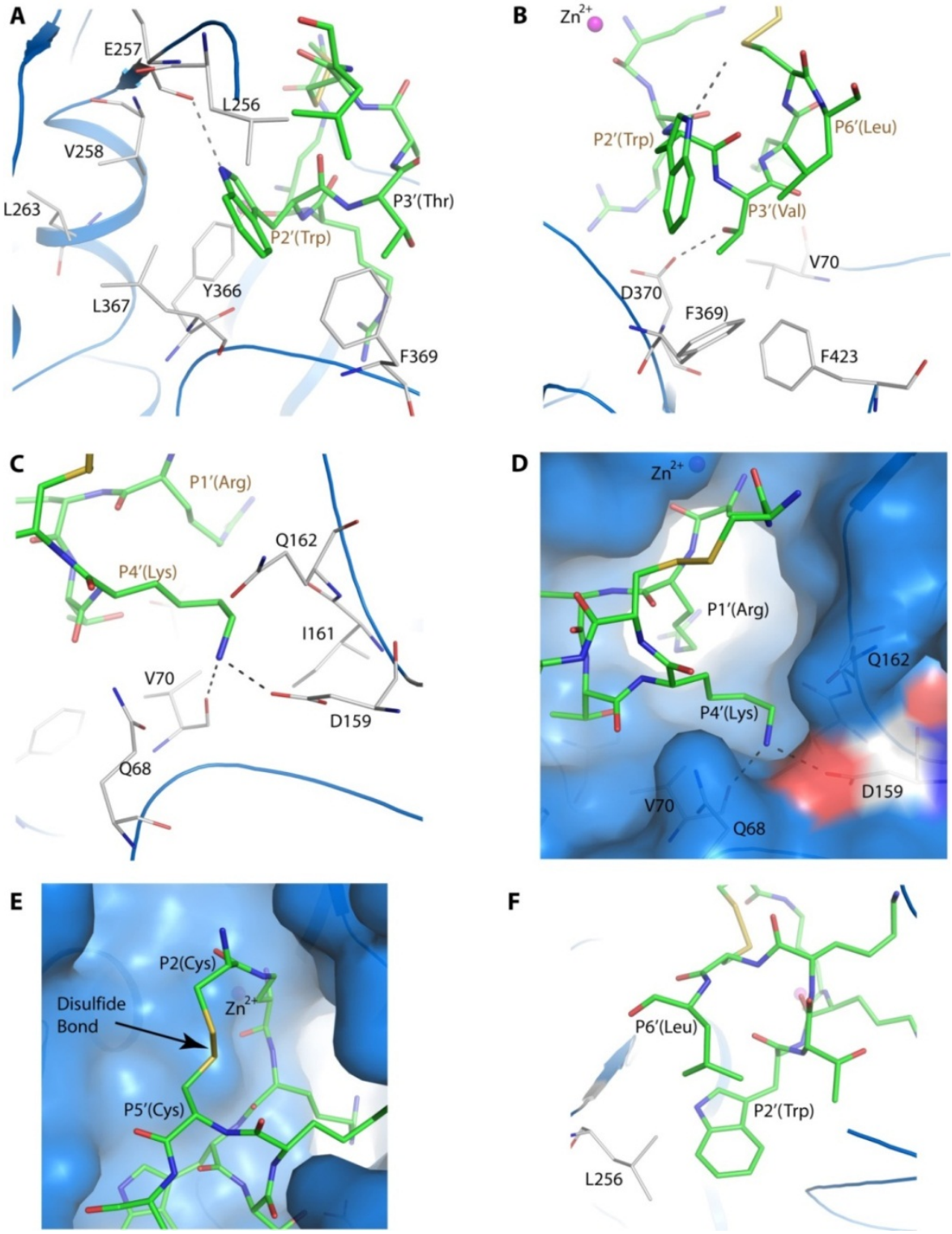
A
E257
L256
V258
L263
P3'(Thr)
P2'(Trp)
Y366
L367
F369
B
Zn2+
P2'(Trp)
P6'(Leu)
P3'(Val)
V70
D370
F369)
F423
C
P1'(Arg)
Q162
P4'(Lys)
I161
V70
D159
Q68
D
Zn2+
P1'(Arg)
Q162
P4'(Lys)
D159
V70
Q68
E
P2(Cys)
Disulfide
Bond
Zn2+
P5'(Cys)
F
P6'(Leu)
P2'(Trp)
L256

Figure 7. Molecular interactions between CPI-1 and Balc424 at the P2′ to P6′ positions. Close-up view of the interactions between CPI-1 and Balc424 at the P2′, P3′, P4′, P4′, P5′ and P6′ positions are shown in panels **(A), (B), (C), (D), (E)** and **(F)**, respectively. V245 has been omitted in figure **(7A)** for clarity. The bonds and carbon atoms of CPI-1 and enzyme residues are shown in green and grey, respectively. Magenta, red, blue and yellow colors represent zinc, oxygen, nitrogen and sulfur atoms, respectively. In panels **(D)** and **(E)**, the active site cavity of Balc424 is shown as surface representation embedded with its secondary structural elements. The negatively charged patch in Balc424 involved in salt bridge interaction is displayed as a red surface.

In the Balc424-CPI-1 complex, the binding interaction of Balc with P4' Lys of the inhibitor is novel. The side chain of P4' Lys binds in the shallow cleft formed by Balc424 residues Q68, V70, I161 and Q162 and engages in the salt bridge interaction with D159. In addition, the side chain of P4' Lys forms a hydrogen bond with the backbone carbonyl oxygen of V70 (Figures 7C & 7D). In the Balc424-QRATKM complex, the P4' Lys is solvent-exposed and proposed to form a hydrogen bond with Q162.[22] Interestingly, these interactions are absent in the complex structure of Balc-SNAP-$25_{146-202}$.[40] Mutation of K201 to Ala in the substrate analog peptide N-Ac-CRATKML increased the K_i 10-fold,[41] suggesting that P4' Lys is important for inhibitory activity.

In contrast to the other residues of CPI-1, P5' Cys is exposed to the solvent region and does not interact with any of the Balc residues (Figure 7E). However, P5’ Cys forms a disulfide bond with the P2 Cys of CPI-1 and hence is involved in the cyclization of the peptide inhibitor. The P6' Leu of CPI-1 interacts with L256 of Balc424 and also forms intra-molecular hydrophobic

interactions with P2' Trp and P3' Thr of CPI-1 (Figure 7F). These intra-peptide hydrophobic interactions and the disulfide bond are suggested to give internal stability and rigidity to CPI-1. Removal of the P6' Leu increased the K_i of the resulting peptide (designated as CPI-2) from 13.9 ± 1.7 nM to 608 ± 149 nM (Figure 8).

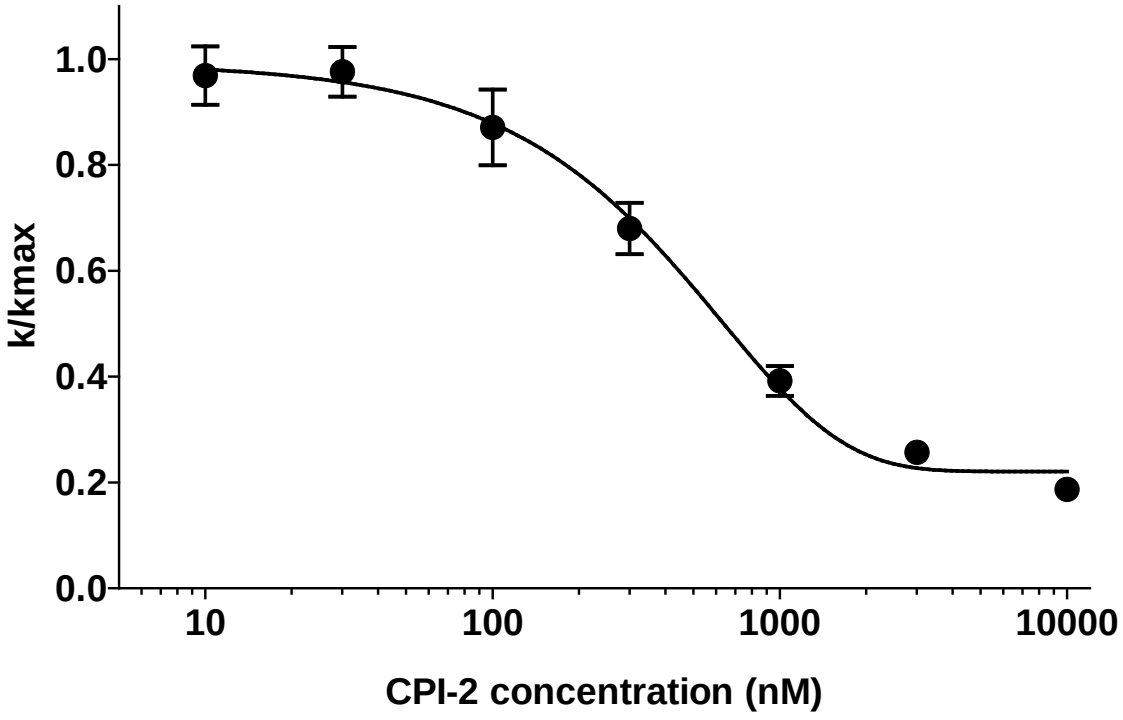

Figure 8. Concentration-response curve for inhibition of Balc448-mediated cleavage of the FRET reporter CFP-SNAP-25(141-206)-YFP. DAB(C)-RWTKC-NH_2 (CPI-2) was incubated with 20 pM Balc448 for 30 min at 37 ^{o}C prior to addition of BoTest® A/E (0.1 μM). The symbols represent the mean ± SEM of 4 experiments. The K_i value for inhibition of Balc448 was 608 ± 149 nM.

3.5. Basis for the Superior Inhibition Potency of CPI-1: Loss of Nucleophilic Water

The Balc active site is characterized by a strictly conserved Zn^{2+} binding motif, HE*XX*H + E, and a catalytic Zn^{2+}. For serotype A, Zn^{2+} is coordinated by H223, E262 and H227. The fourth coordination is provided by a water molecule, which is hydrogen-bonded to E224 and acts as a nucleophile for mediating the proteolytic action of Balc. In the Balc424:CPI-1 complex, this nucleophilic water is replaced by the 2-amino group of DAB, which forms a coordination bond with Zn^{2+} and additionally interacts with E224 (Figure 9A). Therefore, in the inhibited enzyme, there is no nucleophilic water for promoting SNAP-25 proteolysis, leading to inhibition of substrate catalysis. A similar mechanism was also demonstrated in our earlier tetra and hexa peptide inhibitor complexes.[22,28,38]

3.6. Charge Complementarity at the Active Site Cavity

P1' to P6' residues of CPI-1 adopt a 3_{10} left-handed helical conformation in the current complex structure, although analogs to these residues (^{198}RATKM^{202}) form extended beta strands in the Balc:SNAP-25 complex structure.[40] P2' Trp, P3' Thr and P6' Leu of CPI-1 pack against each other through intramolecular hydrophobic interaction and form the hydrophobic side of the helix, whereas P1' Arg and P4' Lys lie on the hydrophilic side. The amphiphilic nature of this helix allows CPI-1 to bind strongly to the Balc active site since charge distribution of the active site cavity of Balc is complementary to that of the inhibitor (Figure 9B).

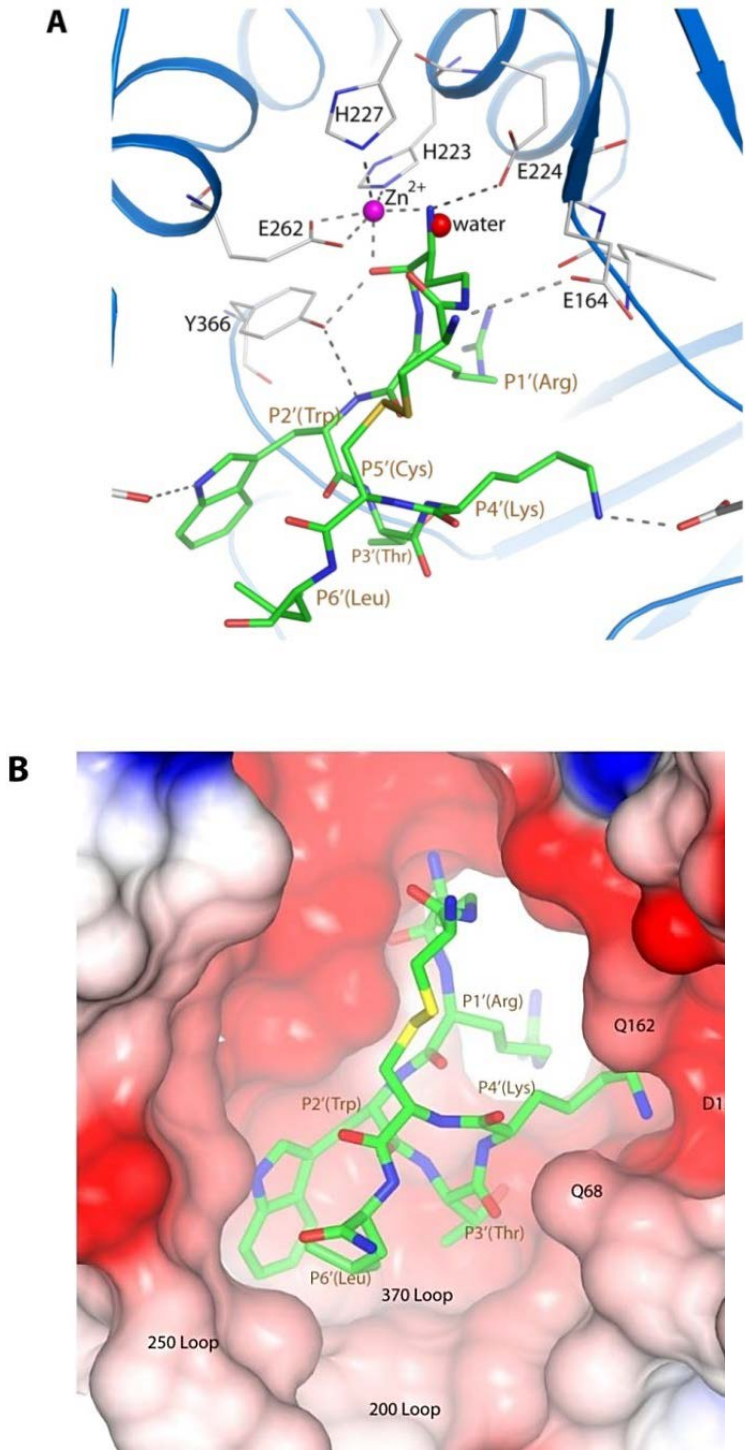

Figure 9. CPI-1 binding to active site of Balc424. **(A)** Complex structure of CPI-1-Balc424 superimposed on native structure of Balc (PDB ID is 2ISH) is displayed. Only the water molecule of native structure is shown for clarity. Balc424 is displayed as

ribbon representation with interacting residues in line form. The bonds and carbon atoms of the CPI-1 and enzyme residues are shown in green and gray, respectively. Zn^{2+} and water are displayed as magenta and red spheres, respectively. **(B)** Electrostatic potential surface representation of active site cavity. CPI-1 is shown in stick model. Red and blue indicate negative (≤ -0.5 V) and positive (≥ + 0.5 V) electrostatic potentials. This figure was prepared with CCP4MG ver 2.8.1.[42]

In the Balc active site cavity, the region near the Zn^{2+} contains a predominantly negative charge, and the region where loops 200, 250 and 370 intersect is hydrophobic. The side chains of P1' Arg and P4' Lys project into the clefts and interact with enzyme residues D370 and D159 through salt bridges (Figure 9B). Hydrophobic residues of CPI-1, viz., P2' Trp, P3' Thr and P6' Leu, pack with the hydrophobic-cum-aromatic pocket formed by the enzyme residues V70, V245, L256, V258, Y366, L367 and F369 (Figure 7). These amphiphilic interactions strengthen the binding affinity of CPI-1 to the Balc424 active site.

3.7. Multi-layer interaction with the active site of Balc424

As shown in Figure 10A, the cyclization of the peptide inhibitor via a disulfide bond in CPI-1 leads to enhanced interactions with the active site of Balc compared to interactions with linear peptide inhibitors.[20,21,24] In addition, CPI-1 fills the active site cavity more completely than the linear peptide inhibitors that we have studied to date, so that access to the active site by SNAP-25 is occluded more completely by CPI. Maintaining the cyclic structure of CPI-1 is vital for

inhibition. Interestingly, the position of cyclization where P2 Cys and P5' Cys form the disulfide bond lies in the entrance of the substrate binding path, thus enabling CPI-1 to effectively block substrate binding (Figure 10B).

A

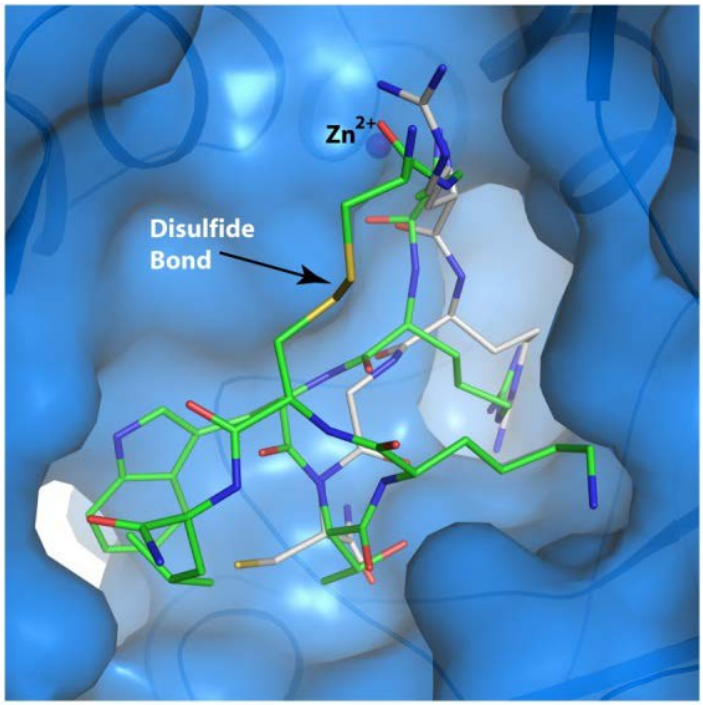

B

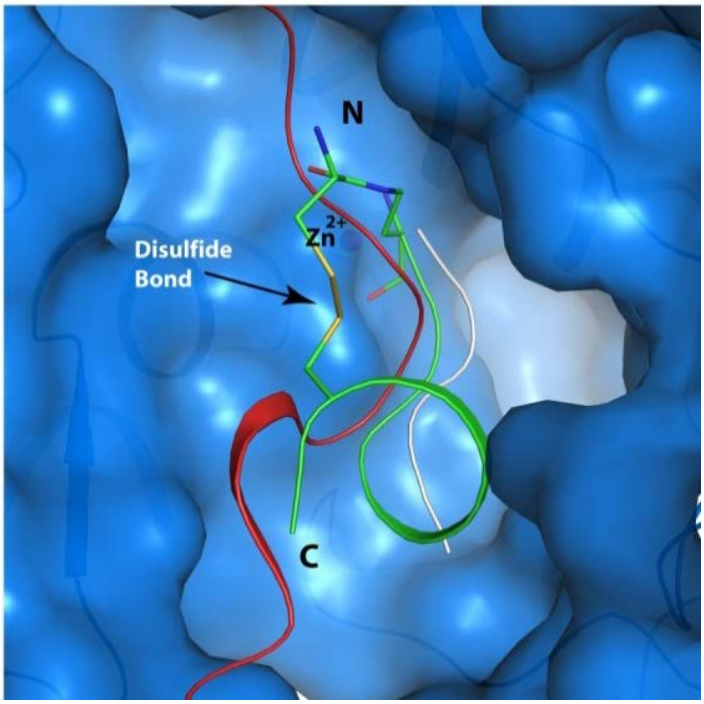

Figure 10. Binding of CPI-1 in the substrate binding cleft of Balc424; the latter is represented as ribbons embedded on the surface model. **(A)** Superposed models (stick) of CPI-1 (green) and peptide RRGC (grey) in the active site cavity of Balc424. **(B)** Superposition of CPI-1 (green), RRGC (grey) and SNAP-25 (red) in the substrate binding cleft of Balc424.

The disulfide bond also gives internal rigidity and stability to the cyclic peptide inhibitor. In this context, it is of interest that inhibition of Balc-mediated proteolysis of BoTest® A/E is reduced over 10-fold when the disulfide bond is cleaved by tris (2-carboxyethyl)phosphine (TCEP) (Table 2). The combined attributes of CPI-1 enable this peptide to inhibit substrate proteolysis more potently than any other inhibitor reported to date.

Due to the poor cell permeability of peptides and their vulnerability to proteolysis,[43] CPI-1 is not expected to have efficacy against BoNT/A in cultured cells or in isolated nerve-muscle preparations. Accordingly, in isolated mouse phrenic nerve-hemidiaphragm preparations exposed to 2.5 pM BoNT/A, co-administration of 15 μM CPI-1 lengthened the half-paralysis time by only 14%. Likewise, in neuron-like cells expressing CFP-SNAP-25-YFP (BoCell® DA), only CPI-1 concentrations ≥100 μM produced significant protection from BoNT/A mediated cleavage of the fluorescent reporter (Adler *et al*., unpublished observations).

A promising solution that retains the advantages of peptide inhibitors is the use hydrocarbon-stapled α-helical peptides. This permits cyclization using an all-hydrocarbon chemical brace to lock the peptide into an active conformation, rather than relying on disulfide bonds which are vulnerable to reduction inside cells. Other advantages of stapling include resistance to proteolysis, increase in serum half-life and cell penetration through endocytic vesicle trafficking.[44]

Table 2. Effect of TCEP (1 mM) on CPI-1-mediated inhibition of Balc448[a]

CPI-1 and TCEP incubated for indicated time and TCEP present during reaction		CPI-1 and TCEP incubated for indicated time but TCEP absent during reaction
Time (min)	K_i (nM)	
30	156.7 ± 22.7[bc]	26.4 ± 5.2[b]
60	161.9 ± 28.6[bc]	46.0 ± 9.1[b]

[a] K_i values determined by FRET assay using BoTest® A/E reporter.

[b] Differs significantly from values in absence of TCEP (13.9 ± 1.7 nM), P<0.01, one-way ANOVA with Bonferroni's pos hoc test.

[c] Differs significantly from samples in which reducing agent was absent during reaction, P< 0.01; unpaired t test, GraphPad Instat v3.06; n = 3 independent determinations, each in triplicate.

4. Conclusions

The cyclic structure generated by the disulfide bond between the P2 and P5' Cys residues of CPI-1 and intramolecular hydrophobic interactions provides internal stability and rigidity to the inhibitor and appears to underlie its high potency. The study presented here is an important milestone and provides critical information for designing more potent peptide and non-peptide inhibitors against the catalytic domain of BoNT/A.

Disclaimer

The views expressed are those of the authors and do not reflect the official policy of the Department of Army, Department of Defense, or U.S. Government. The authors declare no competing financial interests.

Acknowledgments

This work was funded by an award from Defense Threat Reduction Agency Award BO742081 under DOE prime contract No. DEAC02-98CH10886 (SS) and award CB4080 (MA).

The authors would like to thank Dr. Sunil Soni for carrying out NMR studies on CPI-1 and Dr. Leonard Smith for his generous supply of Balc448. We also thank Dr. Brian Molles for his initial contribution to the design of CPI-1.

References

1. Rosetto, O.; Pirazzini, M.; Montecucco, C. *Nat. Rev. Microbiol.* **2014,** *12*, 535.
2. Schiavo, G.; Rosetto, O.; Benfenati, F.; Poulain, B.; Montecucco, C. *Ann. N. Y. Acad. Sci.* **1994,** *710*, 65.
3. Schiavo, G.; Rossetto, O.; Montecucco, C. *Semin. Cell. Biol.* **1994,** *5*, 221.
4. DasGupta, B. R.; Rasmussen, S. *Toxicon* **1983,** *21*, 566.
5. DasGupta, B. R.; Rasmussen, S. *Toxicon* **1983,** *21*, 535.
6. Sathyamoorthy, V.; DasGupta, B. R. *J. Biol. Chem.* **1983,** *260*, 10461.
7. Sathyamoorthy, V.; DasGupta, B. R. *Biochem. Biophys. Res. Commun*. **1985,** *127*, 768.
8. Montecucco, C.; Schiavo, G. *Mol. Microbiol*. **1994,** *13*, 1.
9. Montecucco, C.; Schiavo, G.; Rossetto, O. *Arch. Toxicol. Suppl.* **1996,** *18*, 342.
10. Oguma, K.; Fujinaga, Y.; *Microbiol. Immunol.* **1995,** *39*, 161.
11. Binz, T., Blasi, J.; Yamasaki, S.; Baumeister, A.; Link, E.; Südhof, T. C.; Jahn, R.; *J. Biol. Chem.* **1994,** *269*, 1617.
12. Schiavo, G.; Benfenati, F.; Poulain, B.; Rossetto, O.; Polverino de Laureto, P.; DasGupta, B. R.; Montecucco, C. *Nature* **1992,** *359*, 832.
13. Schiavo, G.; Shone, C. C.; Rossetto, O.; Alexander, F. C.; Montecucco, C.; Schiavo, G. *J. Biol. Chem.* **1993,** *268*, 11516.
14. Schiavo, G.; Rossetto, O.; Catsicas, S.; Polverino de Laureto, P.; DasGupta, B. R.; Benfenati, F.; Montecucco, C. *J. Biol. Chem.* **1993,** *268*, 23784.
15. Schiavo, G.; Malizio, C.; Trimble, W. S.; Polverino de Laureto, P.; Milan, G.; Sugiyama, H.; Johnson, E. A.; Montecucco, C. *J Biol Chem*. **1994,** *269*, 320213.

16. Blasi, J.; Chapman, E. R.; Yamasaki, S.; Binz, T.; Niemann, H.; Jahn, R. *EMBO J.* **1993,** *12*, 4821.

17. Josko, D. *Clin. Lab. Sci.* **2004,** *17*, 30.

18. Cai, S.; Singh, B. R. *Infect. Disord. Drug Targets* **2007,** *7*, 47.

19. Sobel, J. *Clin. Infect. Dis*. **2005,** *41*, 1167.

20. Zuniga, J. E.; Hammill, J. T.; Drory, O.; Nuss, J. E.; Burnett, J. C.; Gussio, R.; Wipf, P.; Bavari, S.; Brunger, A. T. *PLoS One* **2010,** *5*, e11378.

21. Zuniga, J. E.; Schmidt, J. J.; Fenn, T.; Burnett, J. C.; Araç, D.; Gussio, R.; Stafford, R. G.; Badie, S. S.; Bavari, S.; Brunger, A. T. *Structure* **2008,** *16*, 1588.

22. Kumaran, D.; Rawat, R.; Ahmed, S. A.; Swaminathan, S. *PLoS Pathog.* **2008,** *4*, e1000165.

23. Boldt, G.E.; Kennedy, J. P.; Janda, K. D. *Org. Lett.* **2006**, *8***,** 1729.

24. Burnett, J. C.; Ruthel, G.; Stegmann, C. M.; Panchal, R. G.; Nguyen, T. L.; Hermone, A.R.; Stafford, R. G.; Lane, D. J.; Kenny, T. A.; McGrath, C. F.; Wipf, P.; Stahl, A. M.; Schmidt, J. J.; Gussio, R.; Brunger, A. T.; Bavari, S. *J. Biol. Chem.* **2007,** *282, 5004*.

25. Silvaggi, N. R.; Boldt, G. E.; Hixon, M. S.; Kennedy, J. P.; Tzipori, S.; Janda, K. D.; Allen, K. N. *Chem. Biol.* **2007,** *14*, 533.

26. Silvaggi, N. R.; Wilson, D.; Tzipori, S.; Allen, K. N. *Biochemistry* **2008,** *47*, 5736.

27. Park, J. G.; Sill, P. C.; Makiyi, E. F.; Garcia-Sosa, A. T.; Millard, C. B.; Schmidt, J. J.; Pang, Y. P. *Bioorg. Med. Chem.* **2006,** *14*, 395.

28. Kumaran, D.; Rawat, R.; Ludivico, M. L.; Ahmed, S. A.; Swaminathan, S. *J. Biol. Chem.* **2008,** *283*, 18883.

29. Ruge, D. R.; Dunning, F. M.; Piazza, T. M.; Molles, B. E.; Adler, M.; Zeytin, F.N.; Tucker, W. C. *Anal. Biochem.* **2011,** *411*, 2200.

30. Otwinowski, Z.; Minor, W. *Methods Enzymol.* **1997,** *276*, 307.

31. Winn, M. D.; Ballard, C. C.; Cowtan, K. D.; Dodson, E. J.; Emsley, P.; Evans, P. R.; Keegan, R. M.; Krissinel, E. B.; Leslie, A. G.; McCoy, A.; McNicholas, S. J.; Murshudov, G. N.; Pannu, N. S.; Potterton, E. A.; Powell, H. R.; Read, R. J.; Vagin, A.; Wilson, K. S. *Acta Crystallogr. D Biol. Crystallogr.* **2011,** *67*, 235.

32. Murshudov, G. N.; Skubák, P.; Lebedev, A. A.; Pannu, N. S.; Steiner, R. A.; Nicholls, R. A.; Winn, M. D.; Long, F.; Vagin, A. A. *Acta Crystallogr. D Biol. Crystallogr.* **2011,** *67*, 355.

33. Emsley, P.; Lohkamp, B.; Scott, W. G.; Cowtan, K. *Acta Crystallogr. D Biol. Crystallogr.* **2010,** *66*, 486.

34. Laskowski, R. A.; MacArthur, M. W.; Moss, D. S.; Thornton, J. M. *J. Appl. Cryst.* **1993,** *26*, 283.

35. Ahmed, S. A.; Olson, M. A.; Ludivico, M. L.; Gilsdorf, J.; Smith, L. A. *Protein J.* **2008,** *27*, 151.

36. Chen, S.; Kim, J. J.; Barbieri, J. T. Mechanism of substrate recognition by botulinum neurotoxin serotype A. *J. Biol. Chem.* **2007,** *282*, 9627.

37. Binz, T.; Bade, S.; Rummel, A.; Kollewe, A.; Alves, J. *Biochemistry* **2002,** *41*, 1717.

38. Kumar, G.; Kumaran, D.; Ahmed, S. A.; Swaminathan, S. *Acta Crystallogr. D Biol. Crystallogr.* **2012,** *68*, 511.

39. Zuniga, J. E.; Hammill, J. T.; Drory, O.; Nuss, J. E.; Burnett, J. C.; Gussio, R.; Wipf, P.; Bavari, S.; Brunger, A. T. *PLoS One* **2010,** *5*, e11378.

40. Breidenbach, M. A.; Brunger, A. T. *Nature* **2004,** *432*, 925.

41. Schmidt, J. J.; Stafford, R. G. *FEBS Lett.* **2002,** *532*, 423.

42. McNicholas, S.; Potterton, E.; Wilson, K. S.; Noble, M. E. *Acta Crystallogr. D Biol. Crystallogr*. **2011,** *67*, 386.

43. Kim, Y.-W.; Grossmann, T. N.; Verdine, G. L. *Nature Protocols* **2011,** *6*, 761.

44. Verdine, G. L; Hilinski, G. J. *Methods Enzymol*. **2012,** *503*, 3.